

Supporting Information

Synthesis, photophysical and electropolymerization properties of thiophene-substituted 2,3-diphenylbuta-1,3-dienes

Maxime Roger,^a Kassem Amro,^a Joëlle Rault-Berthelot,^b Mathias Quiot,^a Arie Van der Lee,^c Cyril Poriel,^b Sébastien Richeter,^a Sébastien Clément ^{*a} and Philippe Gerbier ^{*a}

- a. ICGM, Univ. Montpellier, CNRS, ENSCM, Montpellier, France.
- b. Univ Rennes, CNRS, ISCR-UMR CNRS 6226, F-35000 Rennes, France.
- c. Institut Européen des Membranes, IEM - UMR 5635, ENSCM, CNRS, Université de Montpellier, Montpellier, France

*To whom correspondence should be addressed: sebastien.clement1@umontpellier.fr,
philippe.gerbier@umontpellier.fr

Table of contents

Figure S1. ^1H NMR spectrum of Sil-T in CD_2Cl_2 .	4
Figure S2. $^{13}\text{C}\{\text{H}\}$ NMR spectrum of Sil-T in CD_2Cl_2	4
Figure S3. $^{29}\text{Si}\{\text{H}\}$ NMR spectrum of Sil-T in CD_2Cl_2 .	5
Figure S4. HR-MS (ASAP) spectrum of Sil-T	5
Figure S5. ^1H NMR spectrum of Sil-BT in CD_2Cl_2 .	6
Figure S6. $^{13}\text{C}\{\text{H}\}$ NMR spectrum of Sil-BT in CD_2Cl_2 .	6
Figure S7. $^{29}\text{Si}\{\text{H}\}$ NMR spectrum of Sil-BT in CD_2Cl_2 .	7
Figure S8. HR-MS (ASAP) spectrum of Sil-BT	7
Figure S9. ^1H NMR spectrum of Sil-EDOT in CD_2Cl_2 .	8
Figure S10. $^{13}\text{C}\{\text{H}\}$ NMR spectrum of Sil-EDOT in CD_2Cl_2 .	8
Figure S11. $^{29}\text{Si}\{\text{H}\}$ NMR spectrum of Sil-EDOT in CD_2Cl_2 .	9
Figure S12. HR-MS (ASAP) spectrum of Sil-EDOT	9
Figure S13. ^1H NMR spectrum of T-DPB in CDCl_3	10
Figure S14. $^{13}\text{C}\{\text{H}\}$ NMR spectrum of T-DPB in CDCl_3 .	10

Figure S15. HR-MS (ASAP) spectrum of T-DPB.	11
Figure S16. ^1H NMR spectrum of BT-DPB in CDCl_3 .	11
Figure S17. $^{13}\text{C}\{\text{H}\}$ NMR spectrum of BT-DPB in CDCl_3 .	12
Figure S18. HR-MS (ASAP) spectrum of BT-DPB.	13
Figure S19. ^1H NMR spectrum of EDOT-DPB in DMSO-d_6 .	13
Figure S20. $^{13}\text{C}\{\text{H}\}$ NMR spectrum of EDOT-DPB in DMSO-d_6 .	13
Figure S21. HR-MS (ASAP) spectrum of EDOT-DPB.	14
Figure S23. ^{29}Si CP/MAS NMR spectrum of A) Sil-T and B) Sil-EDOT	15
Table S1. Crystal and refinement data for Sil-EDOT, T-DPB and BT-DPB.	16
Figure S24. <i>ORTEP</i> style plot of the molecular structure of EDOT-DPB. Note that there is one half-molecule in the asymmetric unit which has completed for this drawing. Atomic displacement ellipsoids are at the 30% probability level.	17
Figure S25. <i>ORTEP</i> style plot of the molecular structure of T-DPB. Note that there are two half-molecules in the asymmetric unit which have completed for this drawing. Atomic displacement ellipsoids are at the 30% probability level.	18
Figure S26. <i>ORTEP</i> style plot of the molecular structure of BT-DPB. Note that there is one half-molecule in the asymmetric unit which has completed for this drawing. Atomic displacement ellipsoids are at the 30% probability level.	19
Figure S27. Determination of optical bandgaps for DPBs	19
Figure S28. Energy and shape of the HOMO (bottom) and LUMO (top)orbitals of optimized structures of Sil-EDOT, as calculated at the B3LYP/6-31+G* level.	20
Figure S29. Energy and shape of the HOMO (bottom) and LUMO (top)orbitals of optimized structures of T-DPB, as calculated at the B3LYP/6-31+G* level.	20
Figure S30 . Energy and shape of the HOMO (bottom) and LUMO (top)orbitals of optimized structures of BT-DPB, as calculated at the B3LYP/6-31+G* level.	21
Figure S31. Energy and shape of the HOMO (bottom) and LUMO (top)orbitals of optimized structures of EDOT-DPB, as calculated at the B3LYP/6-31+G* level.	21
Figure S32. Labelling scheme for relevant structural parameters of the DFT-optimized molecular structures of DPBs	22
Table 2. Relevant structural parameters of the DFT-optimized molecular structures of T-DPB, BT-DPB and EDOT-DPB.	22
Figure S33. Cyclic voltammogram of T-DPB ($5.22 \cdot 10^{-3} \text{ M}$) in $\text{CH}_2\text{Cl}_2 + \text{Bu}_4\text{NPF}_6$ 0.2 M, 100 mV.s^{-1} , Pt disk working electrode. Five recurrent sweeps between -260 and +1180 mV showing the irreversibility of the first oxidation process.	23
Figure S34. Cyclic voltammogram of T-DPB ($5.22 \cdot 10^{-3} \text{ M}$) in $\text{CH}_2\text{Cl}_2 + \text{Bu}_4\text{NPF}_6$ 0.2 M, 100 mV.s^{-1} , Pt disk working electrode. Left: 10 recurrent sweeps between -260 and +1740 mV and Right: 10 recurrent sweeps between -370 and +1860 mV.	23

- Figure S35. Cyclic voltammogram of BT-DPB ($3.95 \cdot 10^{-3}$ M) in $\text{CH}_2\text{Cl}_2 + \text{Bu}_4\text{NPF}_6$ 0.2 M, 100 mV.s^{-1} , Pt disk working electrode. Three recurrent sweeps between 240 and +1040 mV showing the reversibility of the two first oxidation processes. 23
- Figure S36. Cyclic voltammogram of BT-DPB ($3.95 \cdot 10^{-3}$ M) in $\text{CH}_2\text{Cl}_2 + \text{Bu}_4\text{NPF}_6$ 0.2 M, 100 mV.s^{-1} , Pt disk working electrode. Left: 10 recurrent sweeps between 0.24 and +2.05 V and Right: 10 recurrent sweeps between 0.24 and +2.23 V. 24
- Figure S37. Cyclic voltammogram of EDOT-DPB ($3.5 \cdot 10^{-3}$ M) in $\text{CH}_2\text{Cl}_2 + \text{Bu}_4\text{NPF}_6$ 0.2 M, 100 mV.s^{-1} , Pt disk working electrode. Three recurrent sweeps between -760 and +890 mV showing the beginning of electropolymerization since the first oxidation process. 24
- Figure S38. Cyclic voltammogram of EDOT-DPB ($3.5 \cdot 10^{-3}$ M) in $\text{CH}_2\text{Cl}_2 + \text{Bu}_4\text{NPF}_6$ 0.2 M, 100 mV.s^{-1} , Pt disk working electrode. Left: 10 recurrent sweeps between -775 and +1430 mV, Middle: 10 recurrent sweeps between -775 and 1600 mV and Right: 10 recurrent sweeps between -775 and 1980 mV. 24
- References 24

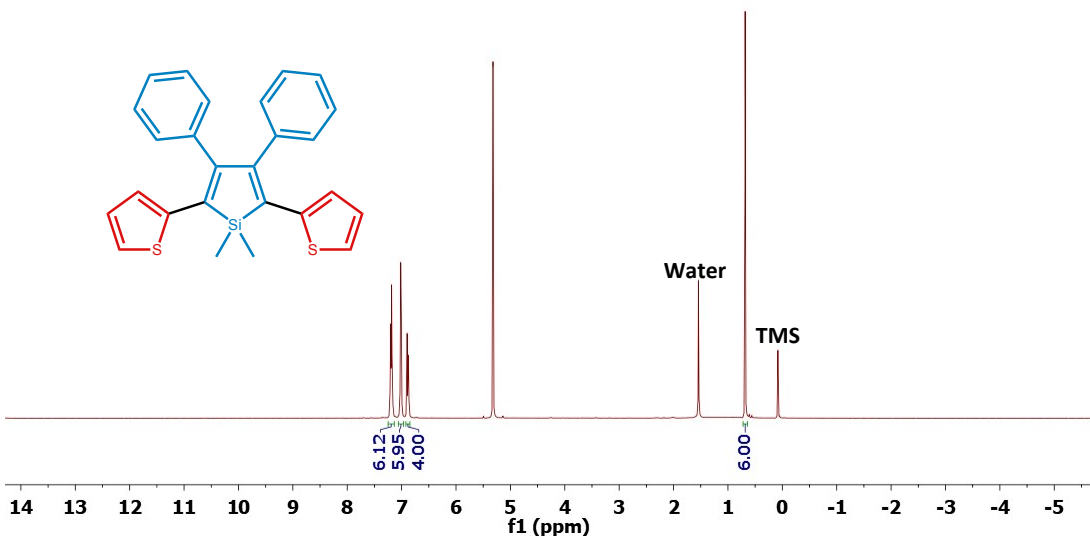


Figure S1. ^1H NMR spectrum of Sil-T in CD_2Cl_2 .

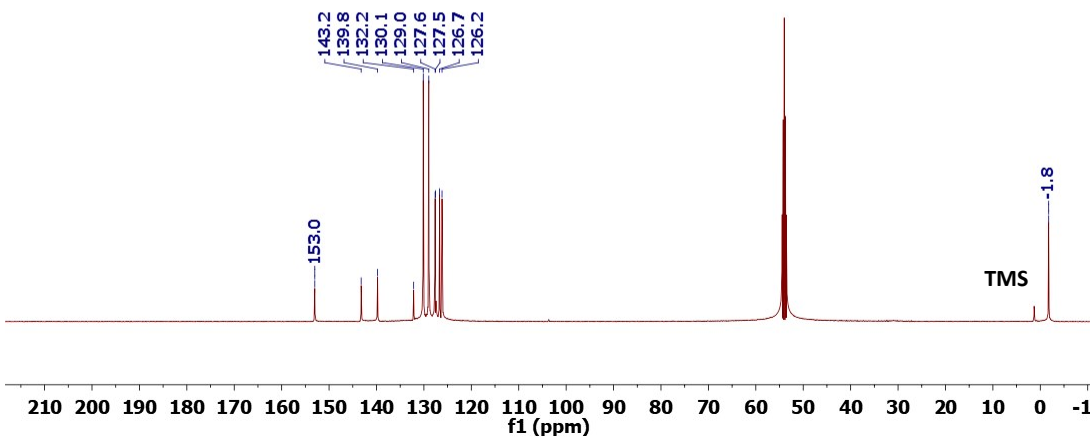


Figure S2. $^{13}\text{C}\{^1\text{H}\}$ NMR spectrum of Sil-T in CD_2Cl_2

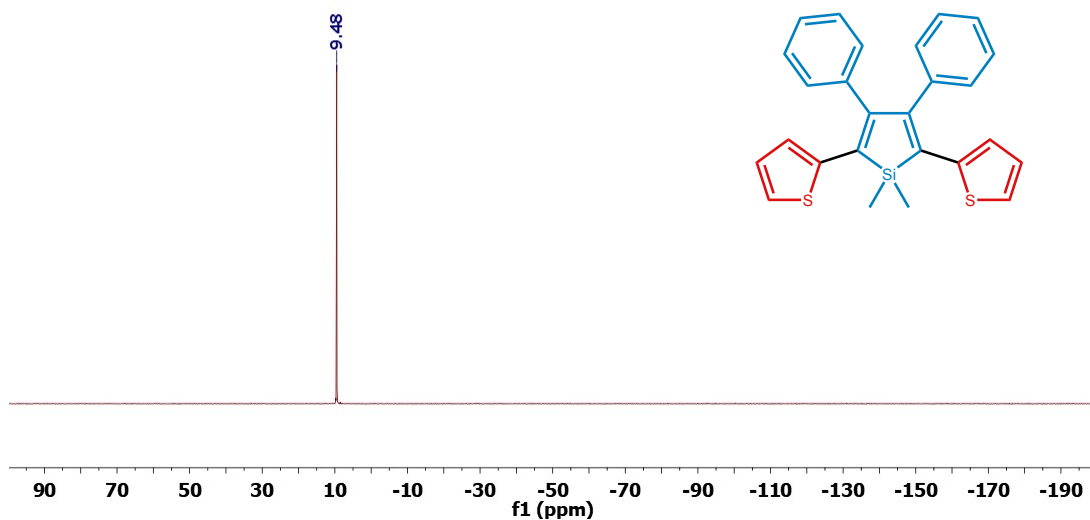


Figure S3. $^{29}\text{Si}\{\text{H}\}$ NMR spectrum of **Sil-T** in CD_2Cl_2 .

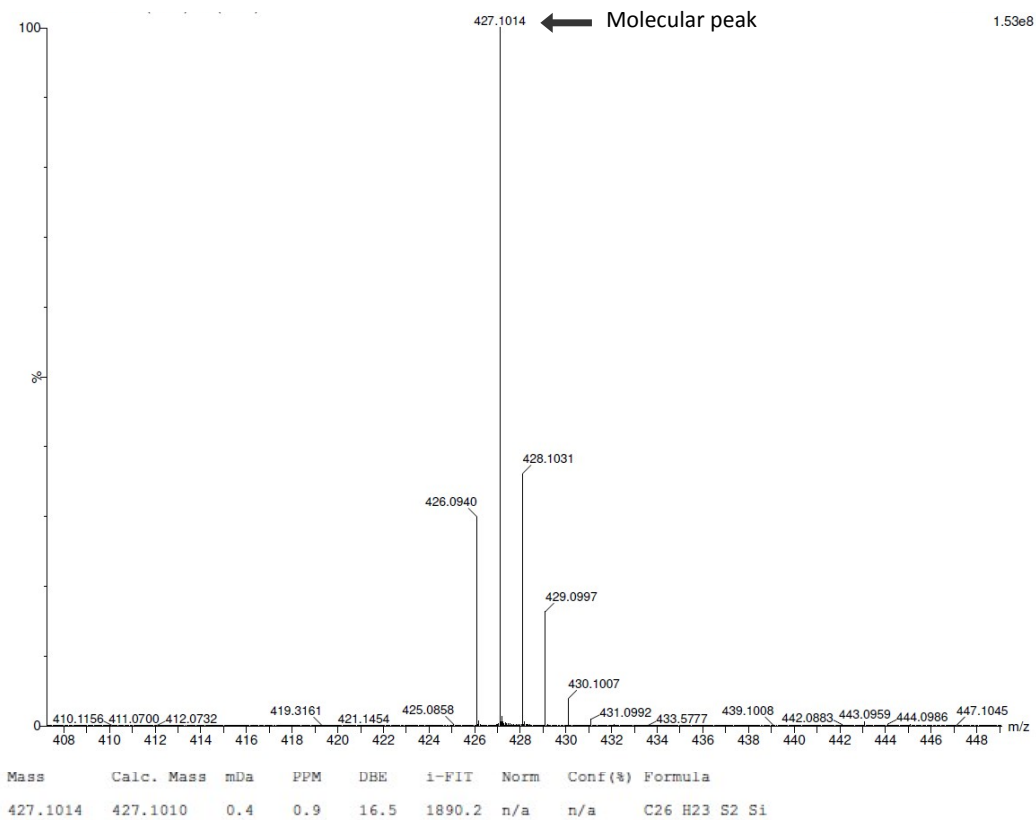


Figure S4. HR-MS (ASAP) spectrum of **Sil-T**

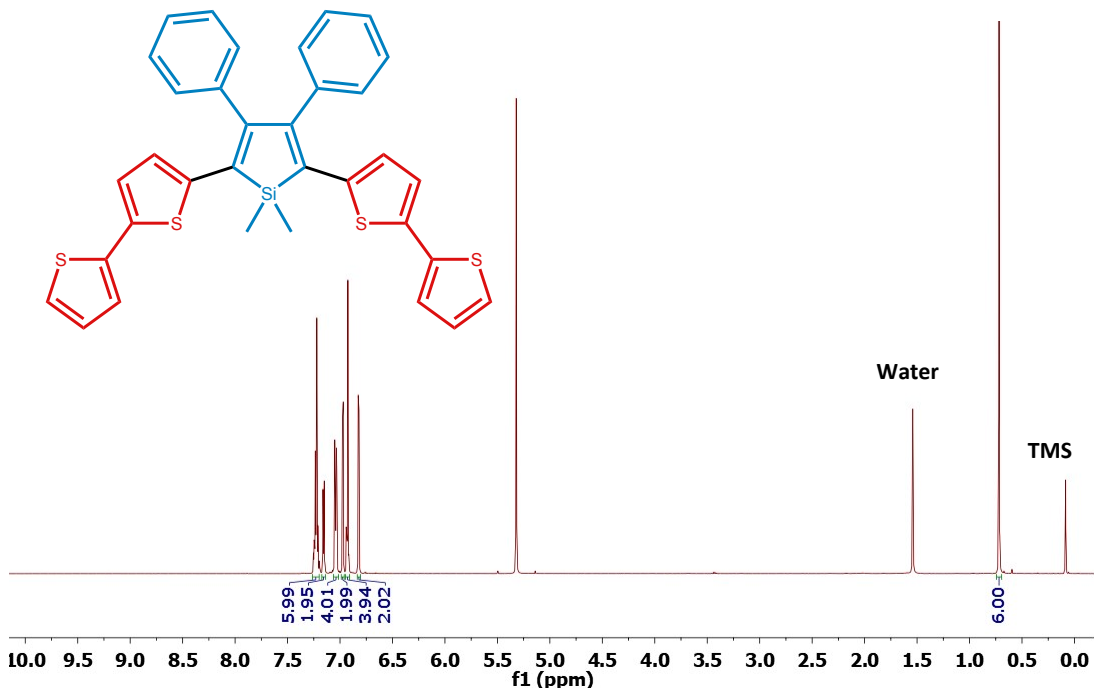


Figure S5. ^1H NMR spectrum of **Sil-BT** in CD_2Cl_2 .

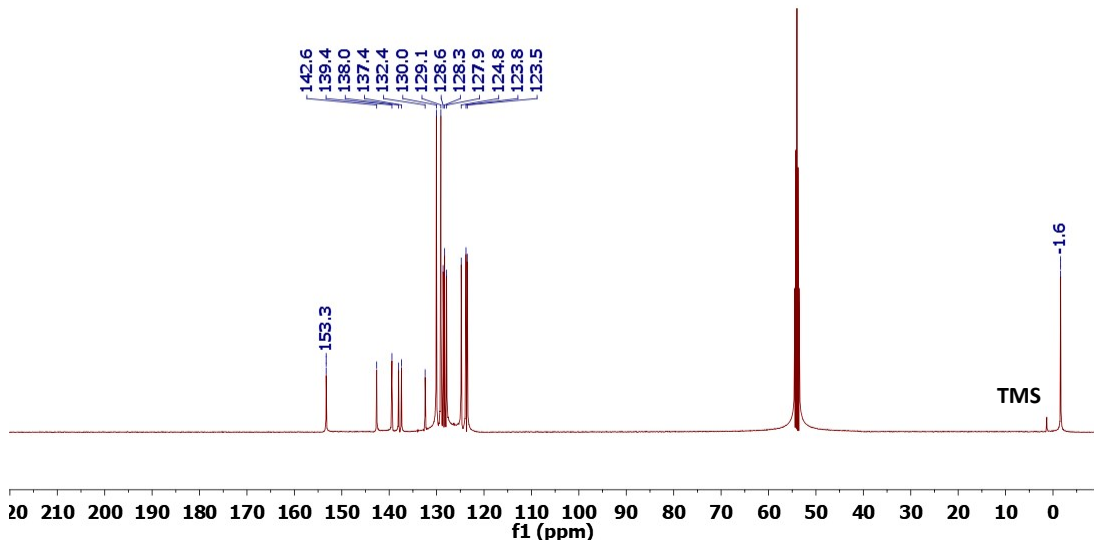


Figure S6. $^{13}\text{C}\{^1\text{H}\}$ NMR spectrum of **Sil-BT** in CD_2Cl_2 .

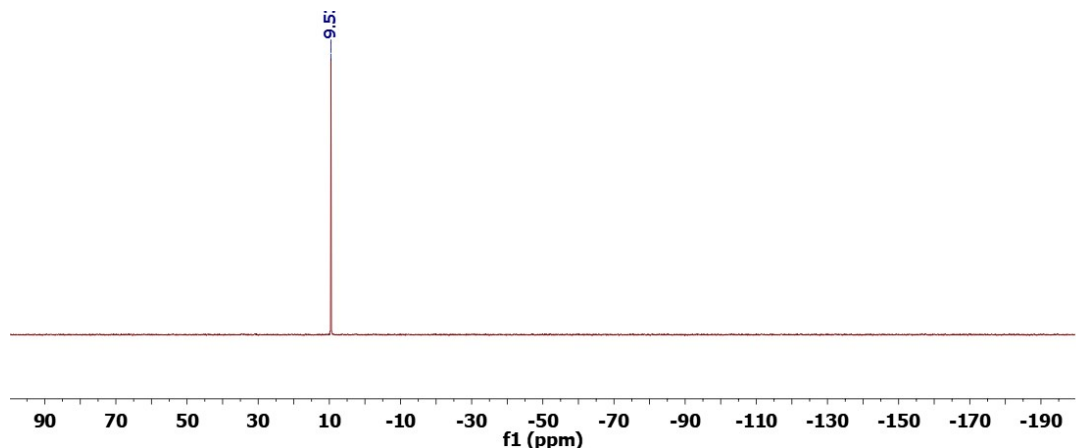


Figure S7. $^{29}\text{Si}\{\text{H}\}$ NMR spectrum of **Sil-BT** in CD_2Cl_2 .

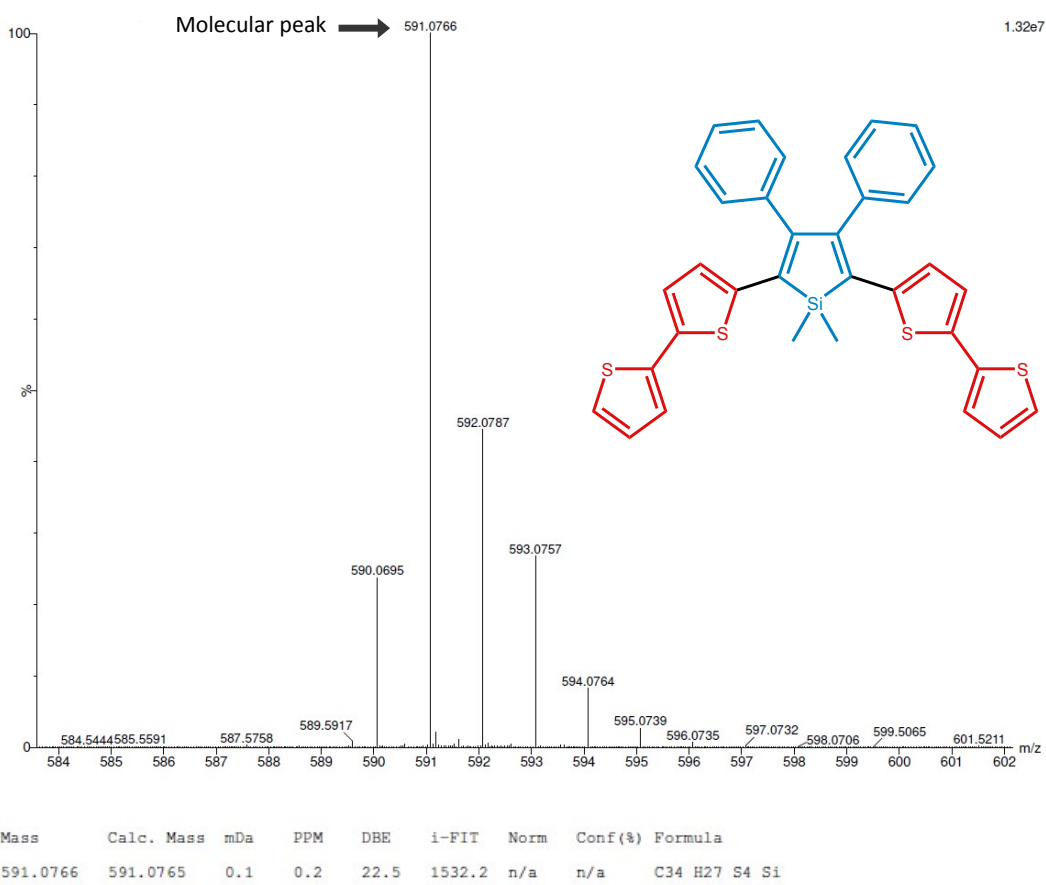


Figure S8. HR-MS (ASAP) spectrum of **Sil-BT**

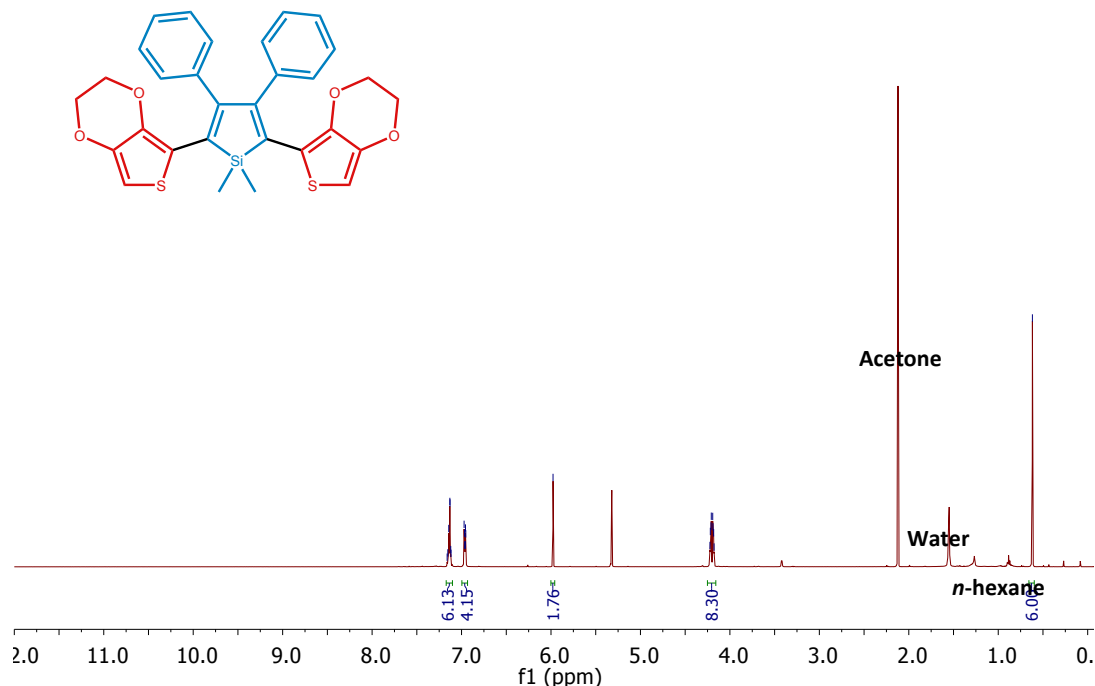


Figure S9. ^1H NMR spectrum of **Sil-EDOT** in CD_2Cl_2 .

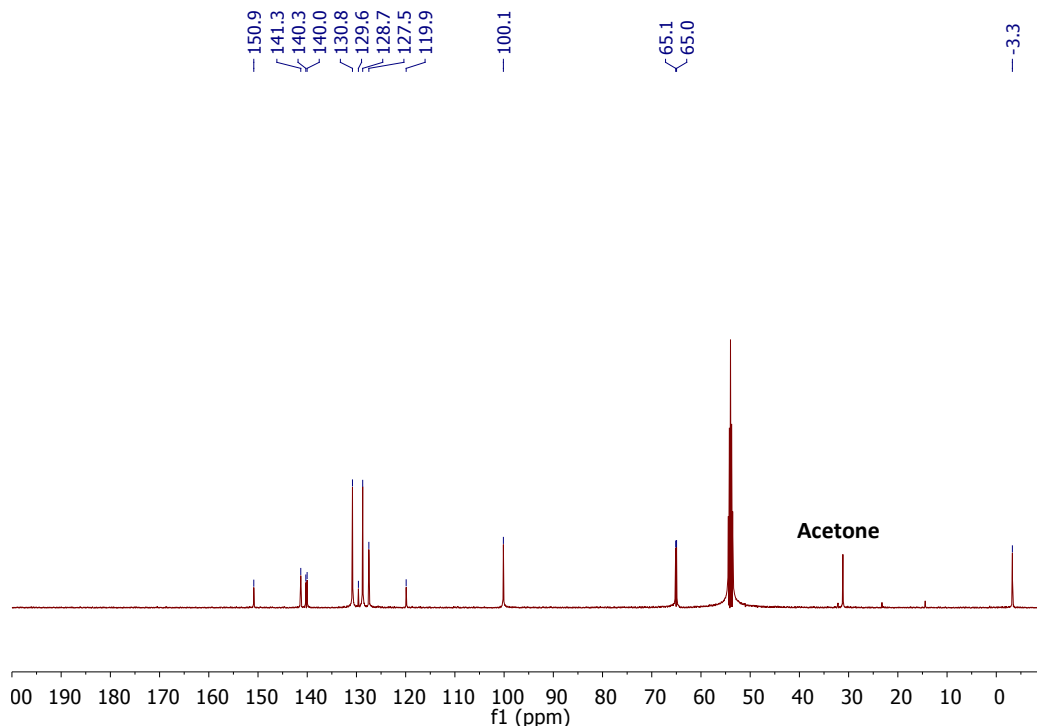
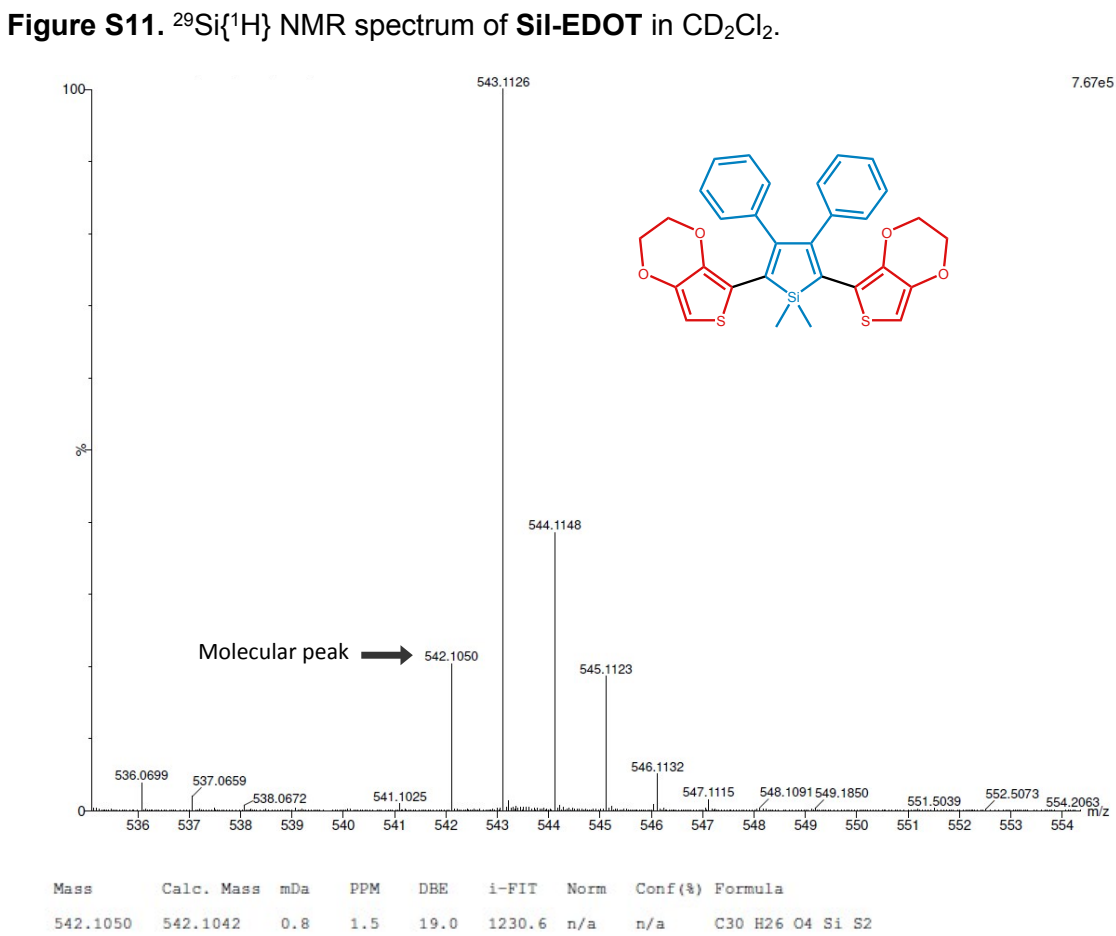
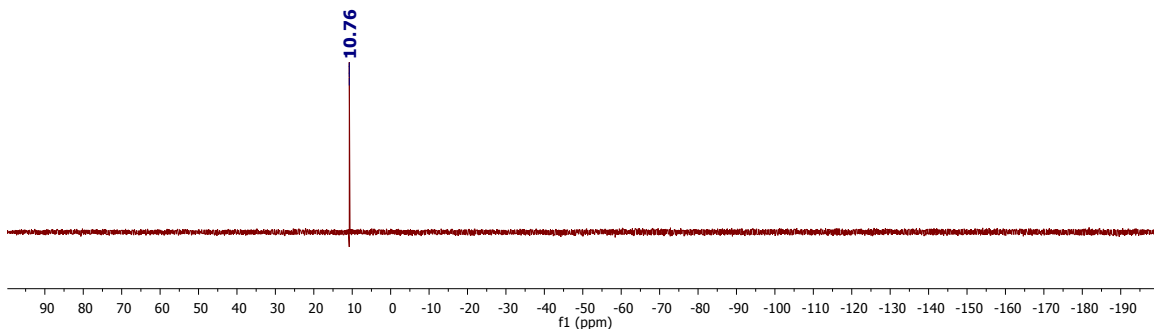


Figure S10. $^{13}\text{C}\{^1\text{H}\}$ NMR spectrum of **Sil-EDOT** in CD_2Cl_2 .



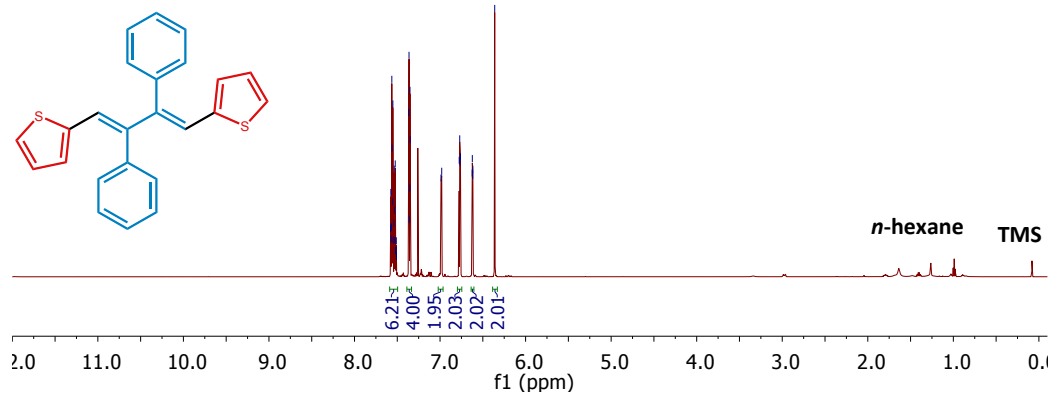


Figure S 13. ^1H NMR spectrum of T-DPB in CDCl_3

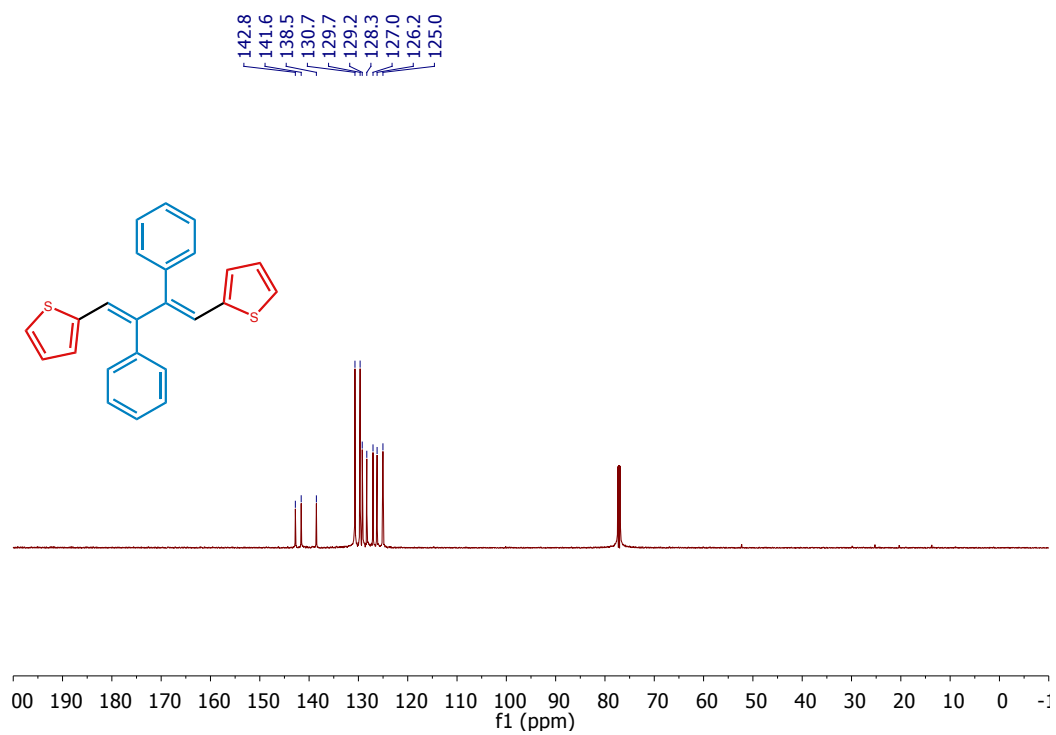


Figure S14. $^{13}\text{C}\{\text{H}\}$ NMR spectrum of T-DPB in CDCl_3 .

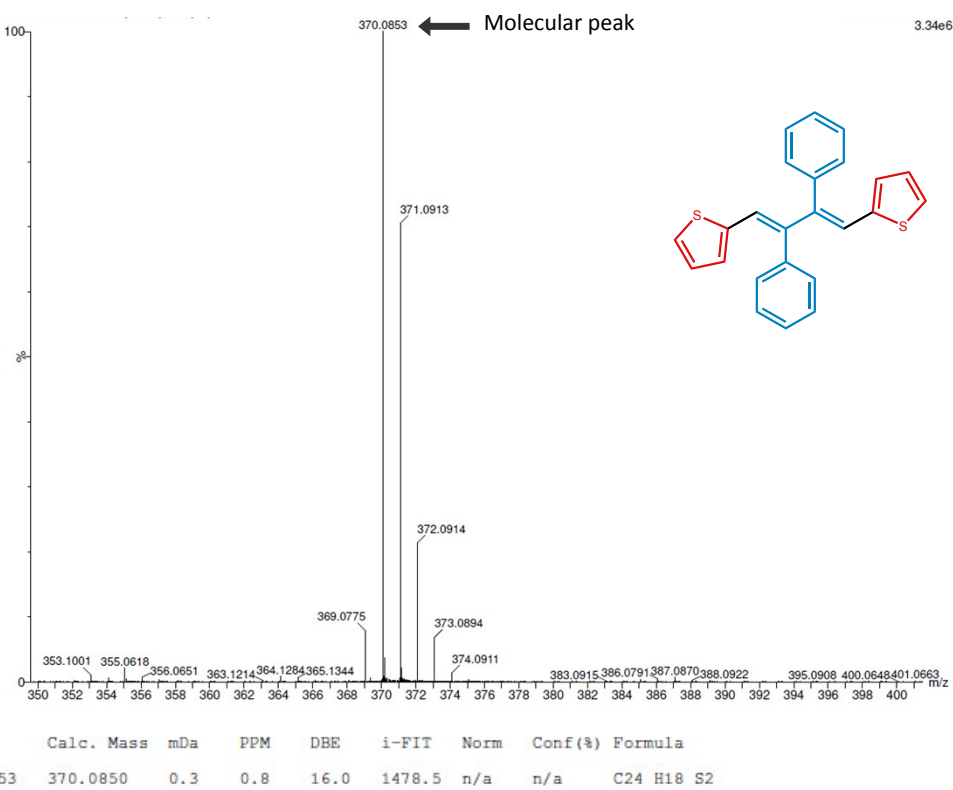


Figure S15. HR-MS (ASAP) spectrum of T-DPB.

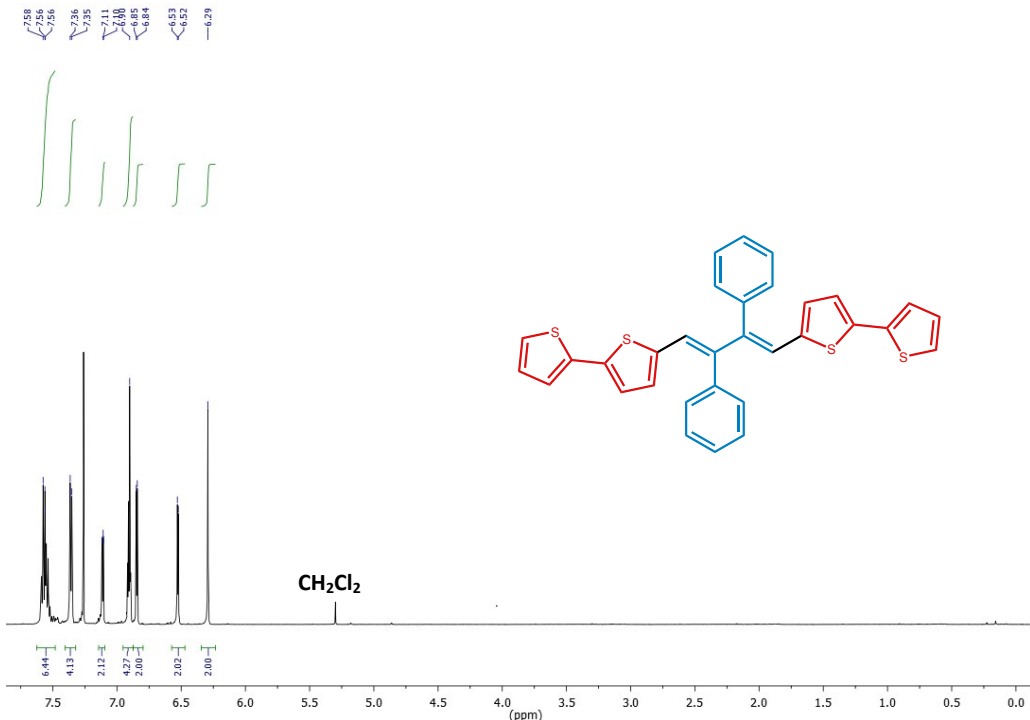


Figure S16. ¹H NMR spectrum of BT-DPB in CDCl₃.

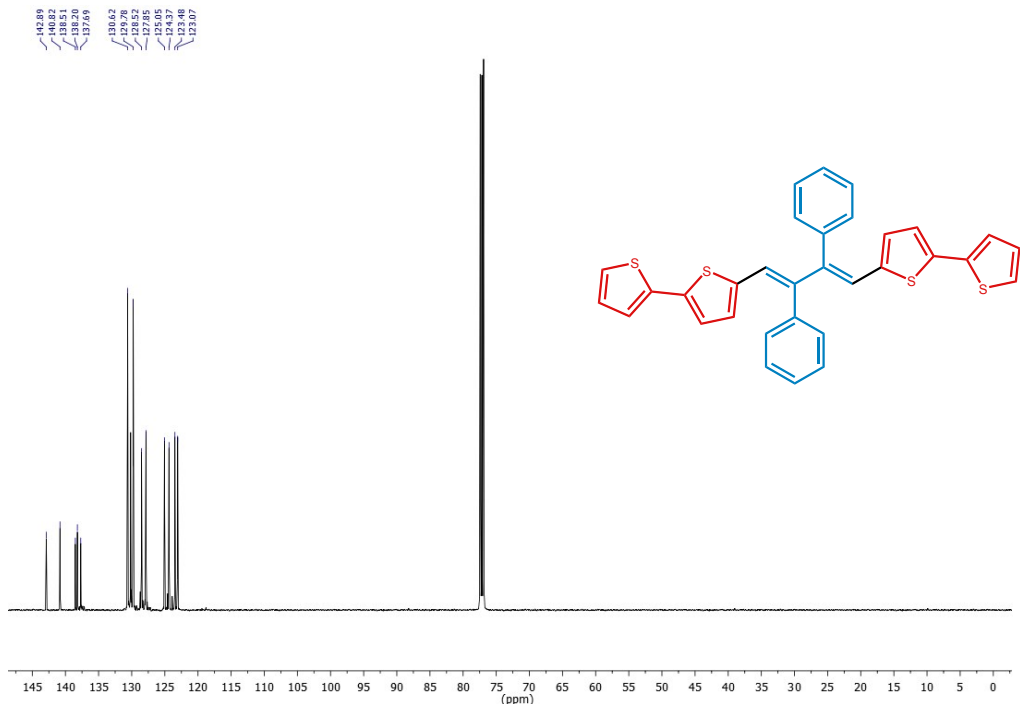


Figure S17. $^{13}\text{C}\{\text{H}\}$ NMR spectrum of **BT-DPB** in CDCl_3 .

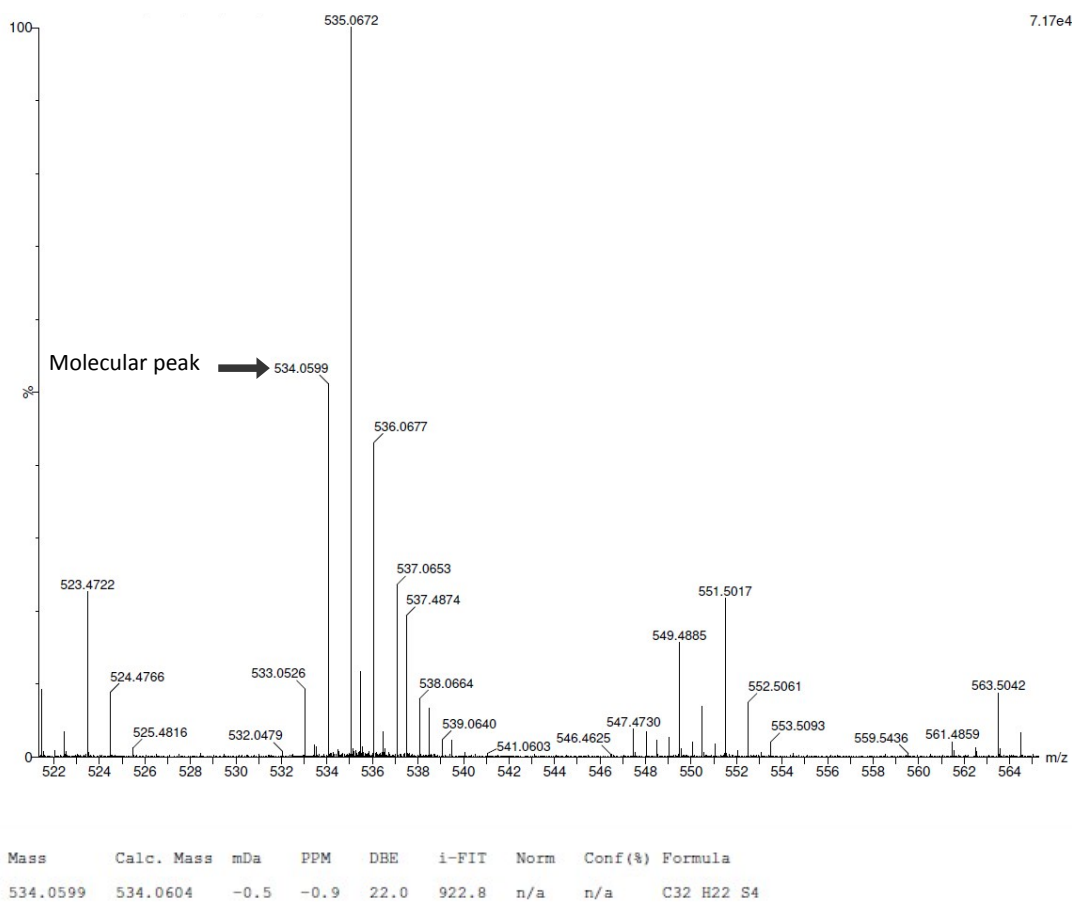


Figure S18. HR-MS (ASAP) spectrum of **BT-DPB**.

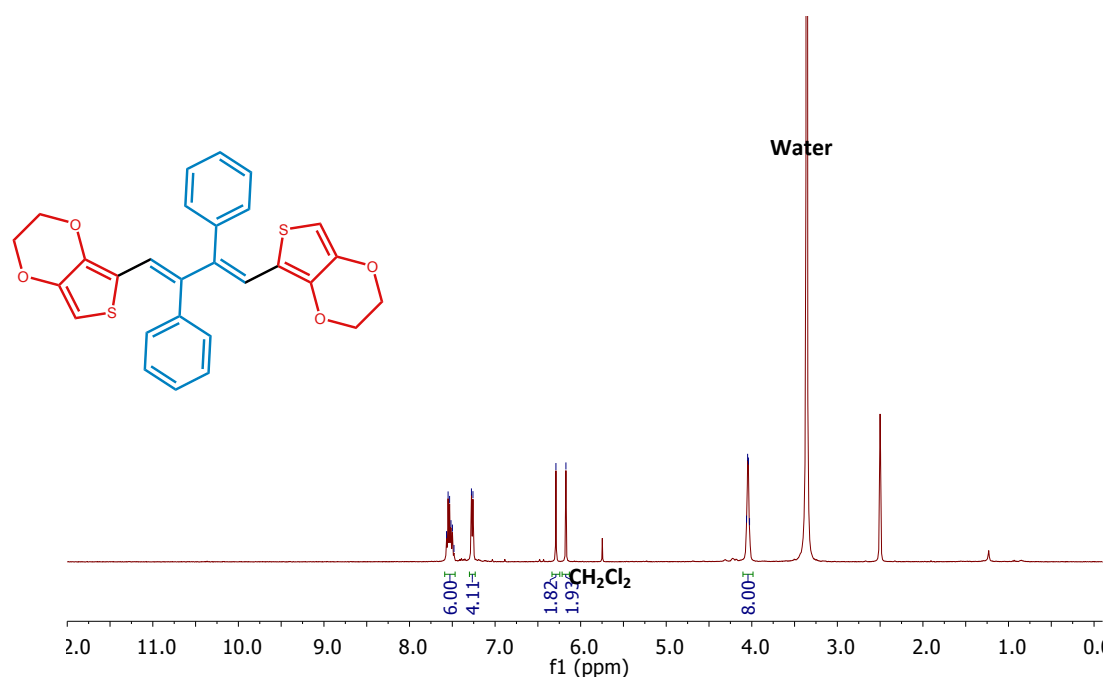


Figure S19. ¹H NMR spectrum of **EDOT-DPB** in DMSO-d₆.

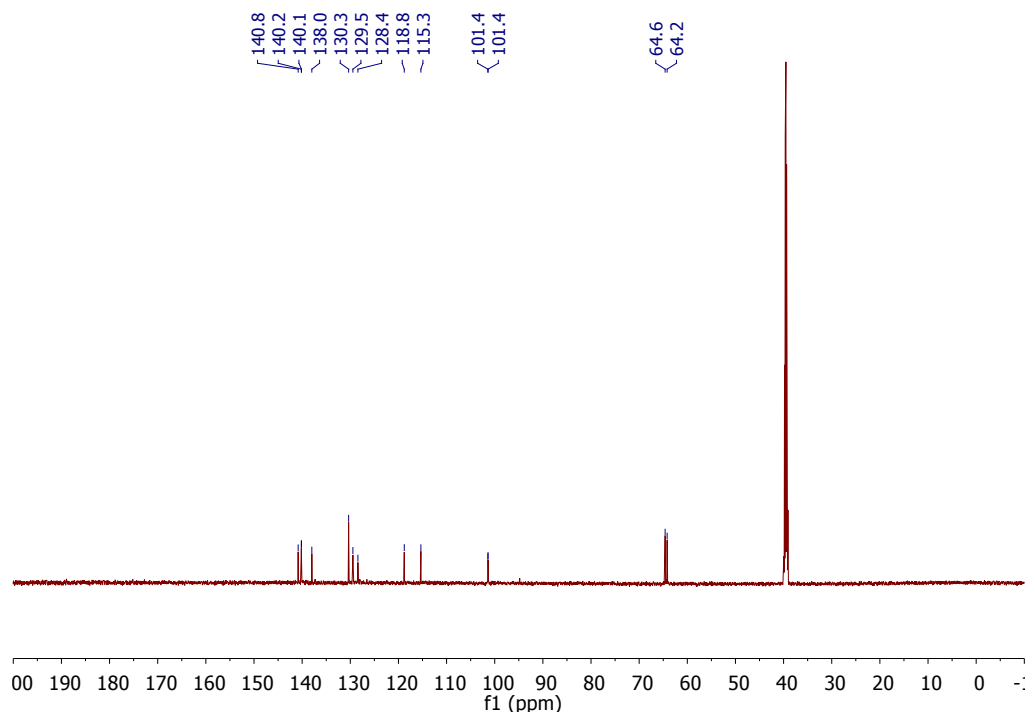


Figure S20. ¹³C{¹H} NMR spectrum of **EDOT-DPB** in DMSO-d₆.

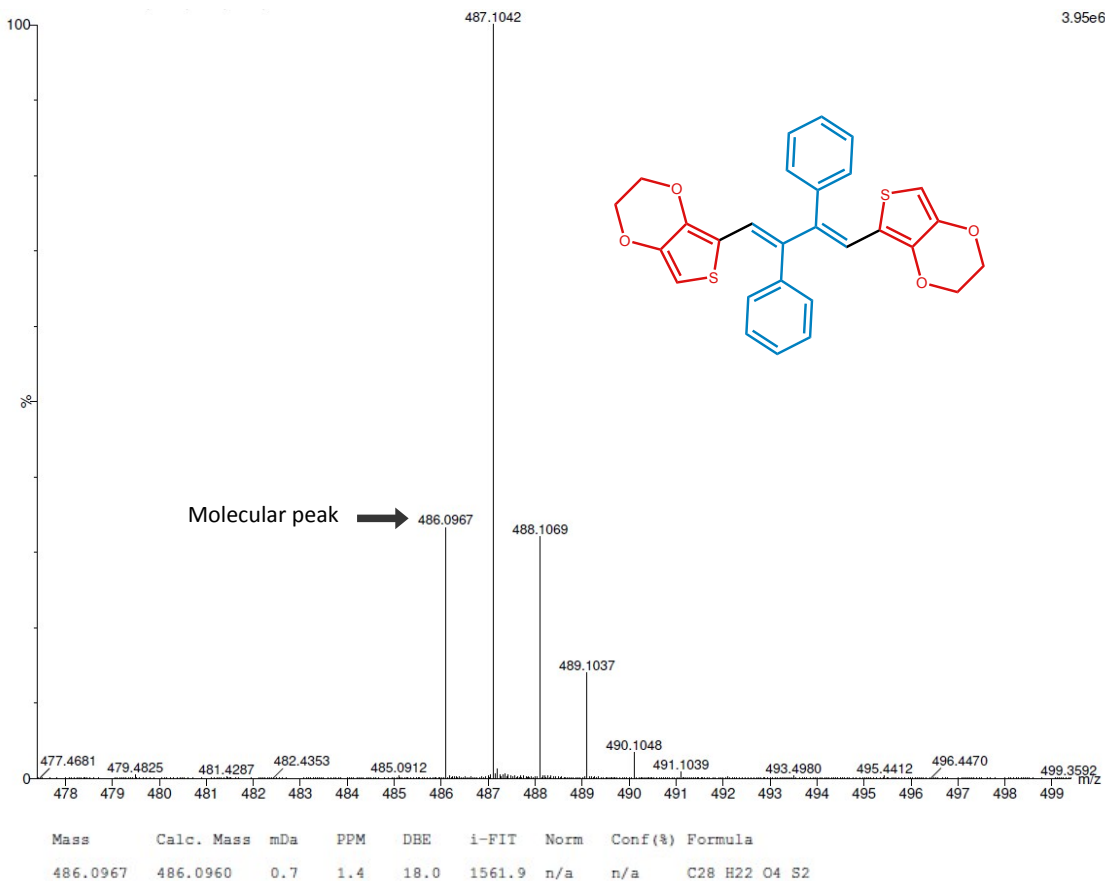


Figure S21. HR-MS (ASAP) spectrum of EDOT-DPB.

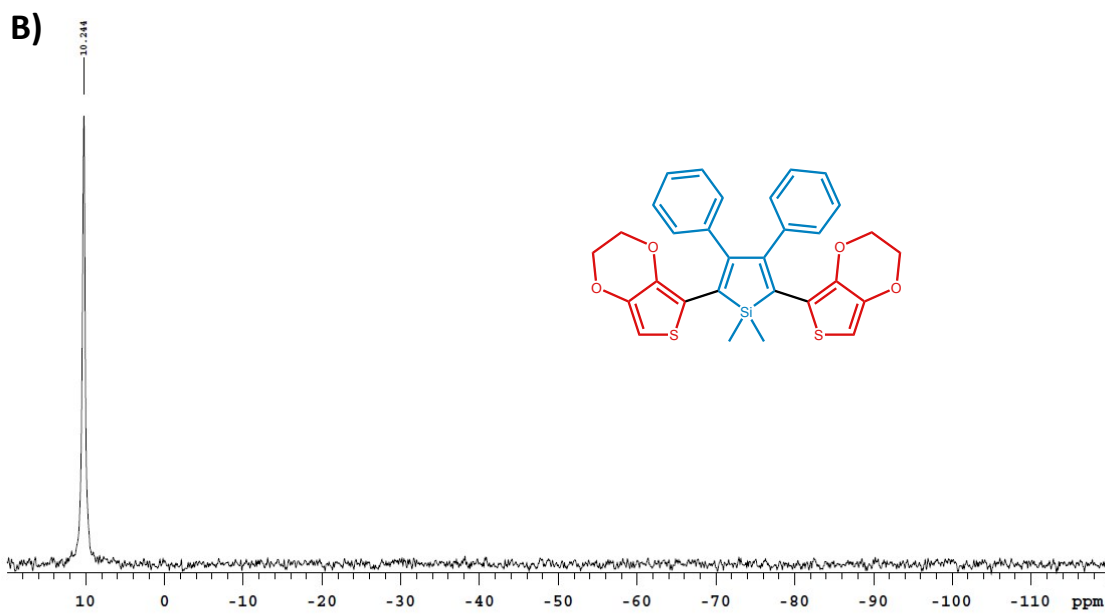
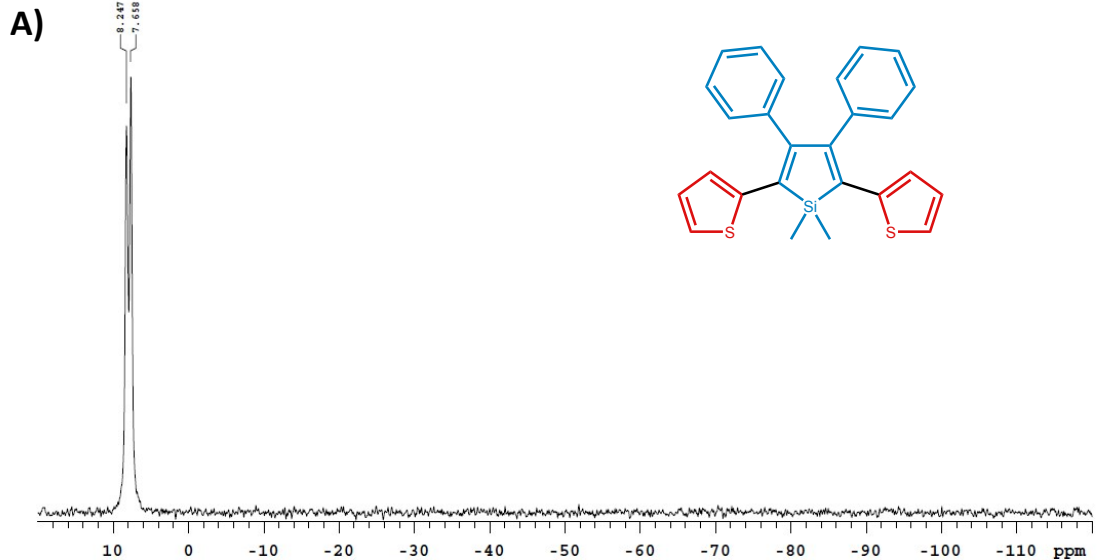


Figure S23. ^{29}Si CP/MAS NMR spectrum of A) SiI-T and B) SiI-EDOT

Table S1. Crystal and refinement data for **Sil-EDOT**, **T-DPB** and **BT-DPB**.

	T-DPB	BT-DPB	EDOT-DPB
formula	C ₂₄ H ₁₈ S ₂	C ₃₂ H ₂₂ S ₄	C ₃₀ H ₂₆ O ₄ S ₂ Si
moiety	C ₂₄ H ₁₈ S ₂	C ₃₂ H ₂₂ S ₄	C ₃₀ H ₂₆ O ₄ S ₂ Si
T (K)	173	173	175
spacegroup	<i>P</i> -1	<i>P</i> 2 ₁ / <i>n</i>	<i>Pnma</i>
crystal system	triclinic	monoclinic	orthorhombic
a (Å)	8.974979(18)	8.343981(17)	9.7622(5)
b (Å)	9.87642(2)	5.578950(13)	22.7394(10)
c (Å)	11.38296(2)	27.61589(3)	11.8095(6)
α (°)	100.050(3)	90	90
β (°)	98.367(3)	98.345(3)	90
γ (°)	104.414(3)	90	90
V (Å³)	943.16(2)	1271.928(12)	2621.5(2)
Z	2	2	4
ρ (gcm⁻³)	1.305	1.396	1.385
M_r (gmol⁻¹)	370.50	534.74	546.69
μ (mm⁻¹)	0.287	0.395	0.318
R_{int}	0.021	0.026	0.0430
Θ_{max} (°)	28.881	27.715	29.213
resolution (Å)	0.74	0.76	0.80
N_{tot} (measured)	12007	12735	9934
N_{ref} (unique)	4344	2569	3126
N_{ref} (I>2σ(I))	3645	2160	2140
N_{ref} (least-squares)	4343	2568	2140
N_{par}	235	163	193
<σ(I)/I>	0.0299	0.033	0.0692
R₁ (I>2σ(I))	0.0361	0.0378	0.0519
wR₂ (I>2σ(I))	0.0853	0.0764	0.0432
R₁ (all)	0.0472	0.0510	0.0519
wR₂ (all)	0.0931	0.0931	0.1269
GOF	0.9956	1.1203	1.3414
Δρ (eÅ⁻³)	-0.44/0.43	-0.48/0.47	-0.94/0.33
crystal size (mm³)	0.05x0.10x0.15	0.03x0.08x0.25	0.02x0.07x0.15

Crystal structures. X-ray diffraction data of the structures have been measured on a Rigaku Oxford Diffraction Xcalibur four circle diffractometer using Mo- $K\alpha$ radiation ($\lambda = 0.71073 \text{ \AA}$) equipped with a Sapphire2 detector at 175 K. The structures have been solved using the *ab initio* charge flipping method as implemented in SUPERFLIP.¹ The crystal of structure of EDOT-DPB showed disorder in the dioxane group for two carbon atoms. The refined relative occupancies were 0.717/0.283. In this structure, geometrical and atomic displacement restraints were used to keep the disordered parts chemically reasonable.

Hydrogen atom positions were determined using Fourier differential maps. All structures were initially refined using non-linear least-squares methods as implemented in CRYSTALS,² in which the hydrogen atoms were treated as riding on their parent atoms and with $U_{\text{iso}}(\text{H})$ constrained to in general 1.2-1.5 times $U_{\text{eq}}(\text{H})$ that of the parent atom. The positions of hydrogen atoms involved in classical hydrogen bonds were refined using geometrical restraints. ORTEP style plots have been made with OLEX2.³

CCDC 1999640 - 1999642 contain the supplementary crystallographic data for this paper. These data can be obtained free of charge from The Cambridge Crystallographic Data Centre via www.ccdc.cam.ac.uk/structures

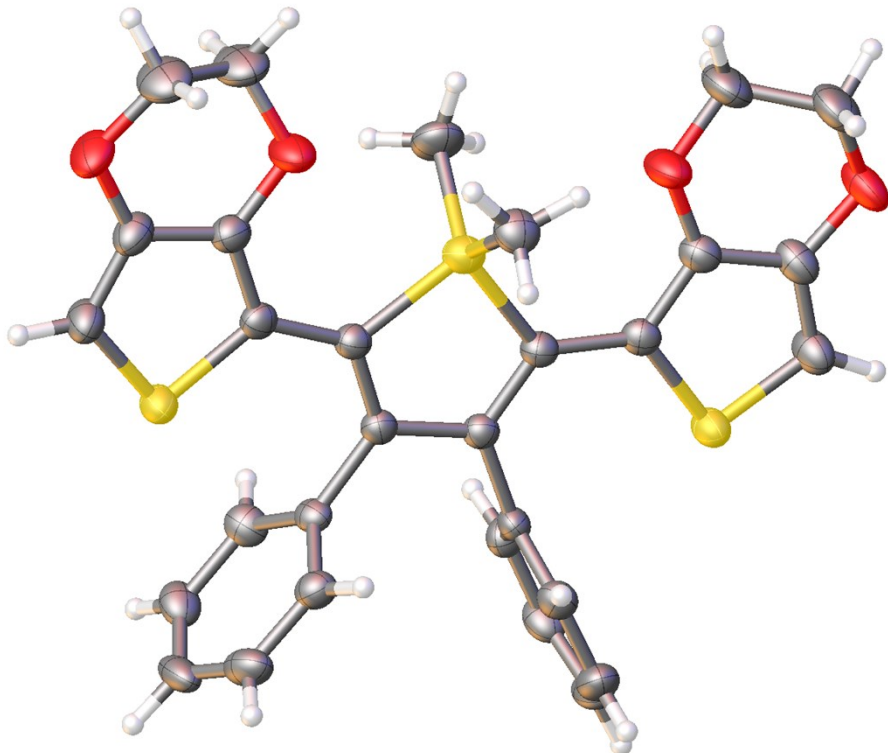


Figure S24. ORTEP style plot of the molecular structure of EDOT-DPB. Note that there is one half-molecule in the asymmetric unit which has completed for this drawing. Atomic displacement ellipsoids are at the 30% probability level.

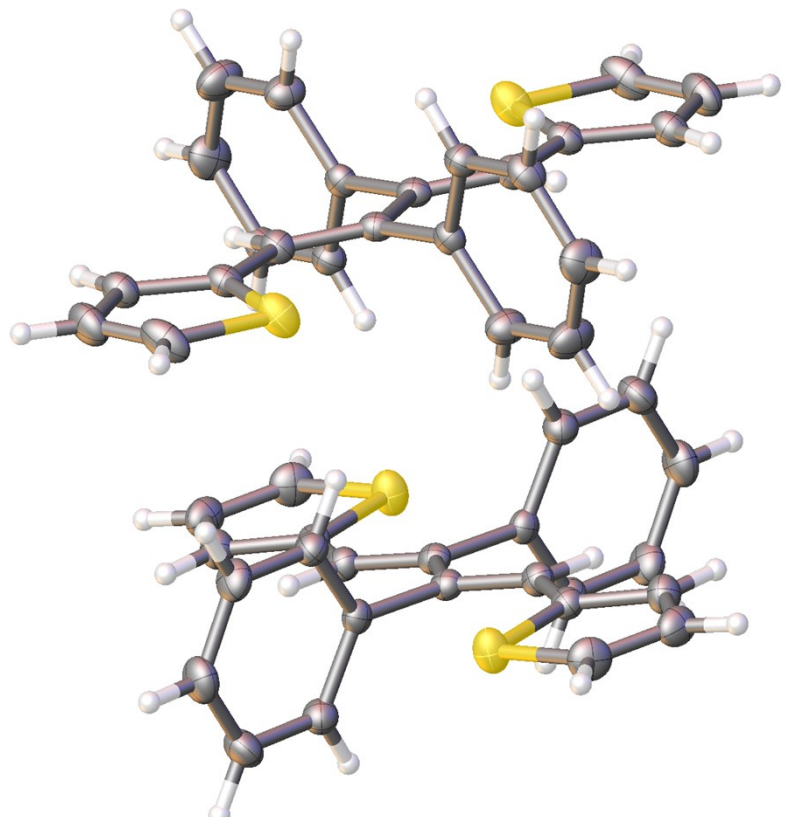


Figure S25. *ORTEP* style plot of the molecular structure of **T-DPB**. Note that there are two half-molecules in the asymmetric unit which have completed for this drawing. Atomic displacement ellipsoids are at the 30% probability level.

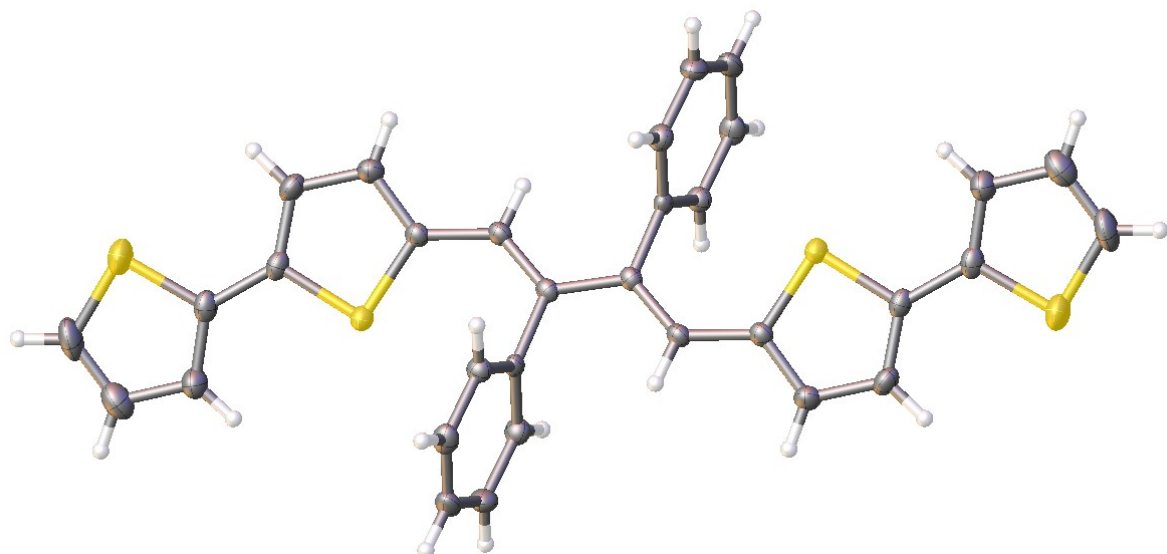


Figure S26. ORTEP style plot of the molecular structure of **BT-DPB**. Note that there is one half-molecule in the asymmetric unit which has completed for this drawing. Atomic displacement ellipsoids are at the 30% probability level.

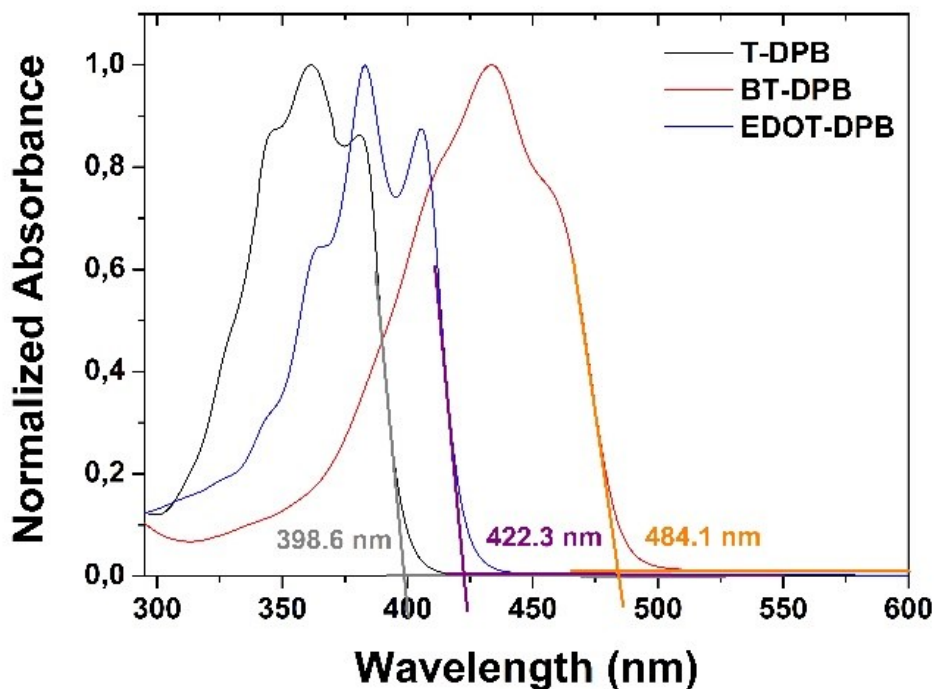


Figure S27. Determination of optical bandgaps for DPBs

Calculations. The electronic structure of all derivatives have been calculated at the DFT (Density Functional Theory) level using the B3LYP⁴ functional and a 6-31+G* basis set on DFT(B3LYP/6-31G)-optimized geometries. All the calculations have been performed within the Gaussian 09 package.⁵

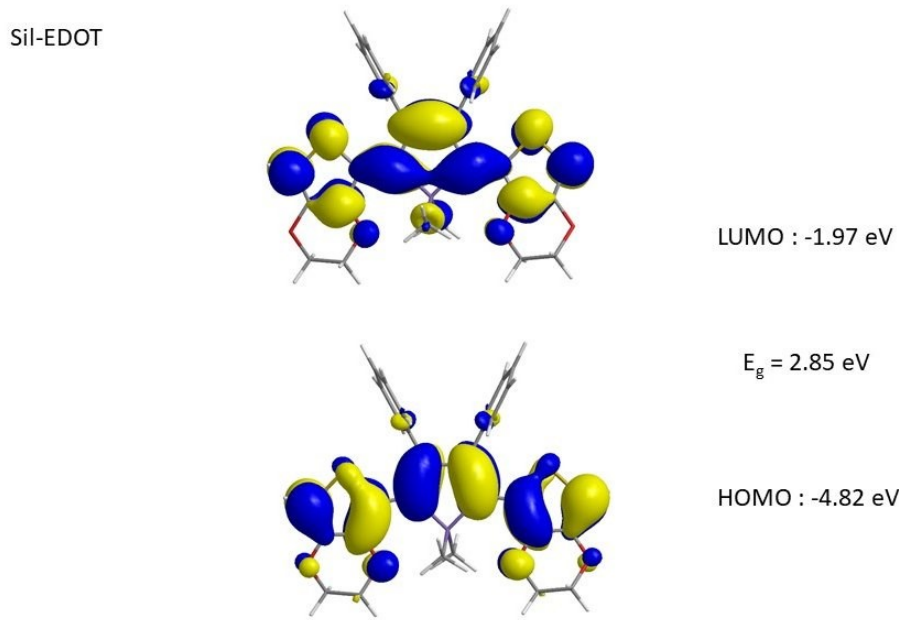


Figure S28. Energy and shape of the HOMO (bottom) and LUMO (top)orbitals of optimized structures of **Sil-EDOT**, as calculated at the B3LYP/6-31+G* level.

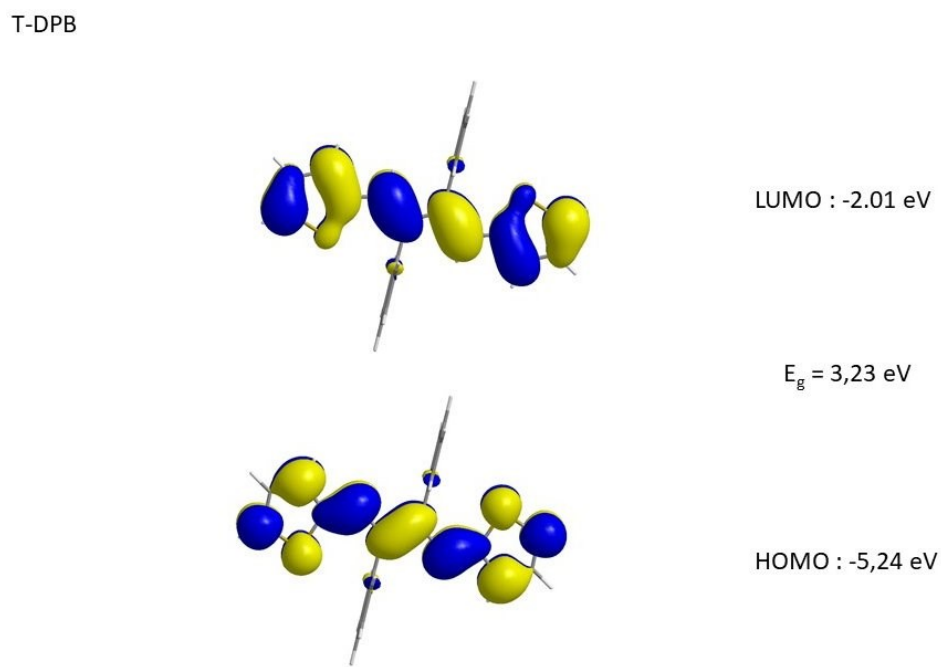


Figure S 29. Energy and shape of the HOMO (bottom) and LUMO (top)orbitals of optimized structures of **T-DPB**, as calculated at the B3LYP/6-31+G* level.

BT-DPB

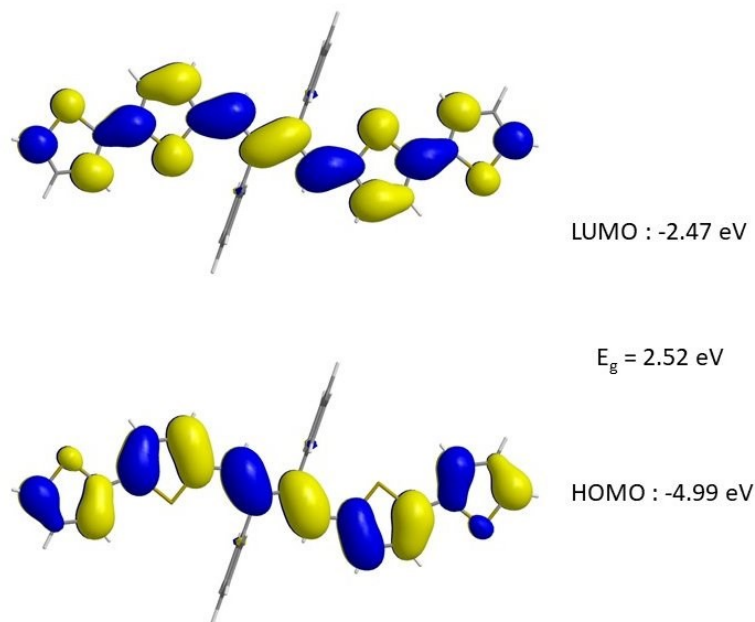


Figure S30 . Energy and shape of the HOMO (bottom) and LUMO (top)orbitals of optimized structures of **BT-DPB**, as calculated at the B3LYP/6-31+G* level.

EDOT-DPB

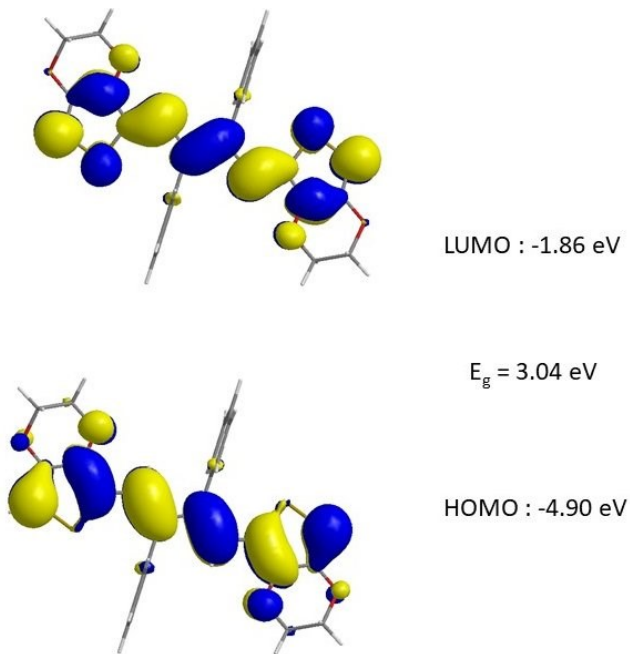


Figure S31. Energy and shape of the HOMO (bottom) and LUMO (top)orbitals of optimized structures of **EDOT-DPB**, as calculated at the B3LYP/6-31+G* level.

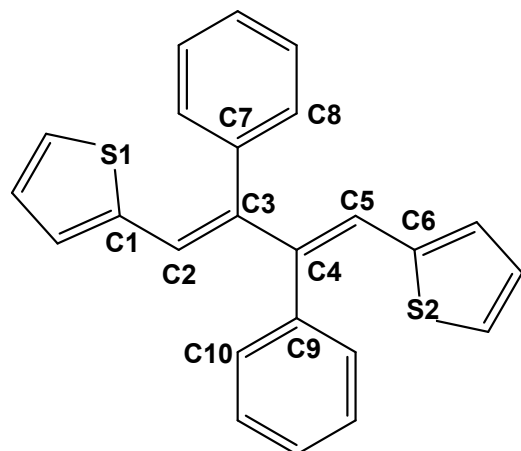


Figure S32. Labelling scheme for relevant structural parameters of the DFT-optimized molecular structures of **DPBs**

Table 2. Relevant structural parameters of the DFT-optimized molecular structures of **T-DPB**, **BT-DBP** and **EDOT-DPB**.

	T-DPB	BT-DBP-	EDOT-DPB
C1-C2	1.44 Å	1.43 Å	1.44 Å
C2-C3	1.37 Å	1.37 Å	1.37 Å
C3-C4	1.47 Å	1.47 Å	1.48 Å
C4-C5	1.37 Å	1.37 Å	1.37 Å
C5-C6	1.44 Å	1.43 Å	1.44 Å
S1-C1-C2-C3	1.0°	0.0°	2.3°
S2-C6-C5-C4	1.0°	0.0°	2.3°
C2-C3-C7-C8	89.4°	89.5°	86.7°
C5-C4-C9-C10	89.4°	89.5°	86.7°

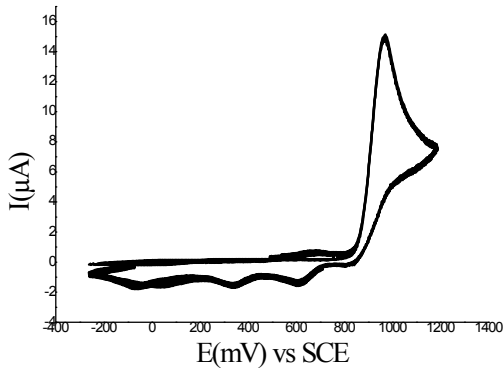


Figure S33. Cyclic voltammogram of **T-DPB** ($5.22 \cdot 10^{-3}$ M) in $\text{CH}_2\text{Cl}_2 + \text{Bu}_4\text{NPF}_6$ 0.2 M, 100 mV.s^{-1} , Pt disk working electrode. Five recurrent sweeps between -260 and +1180 mV showing the irreversibility of the first oxidation process.

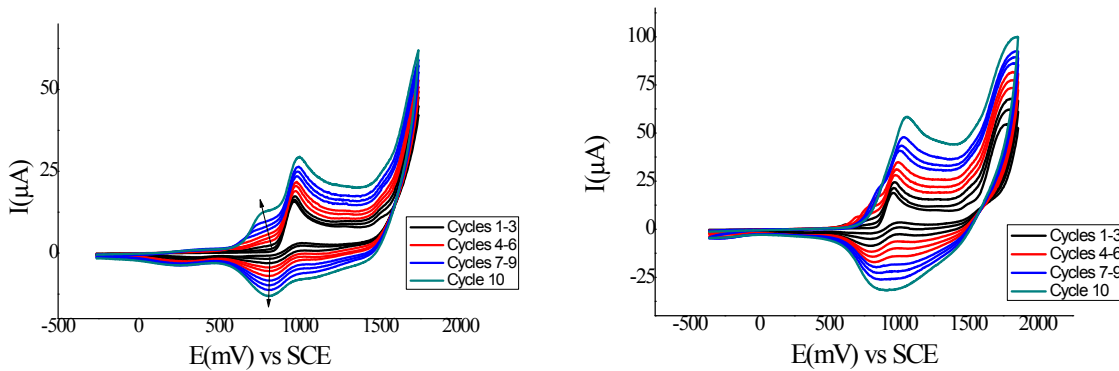


Figure S34. Cyclic voltammogram of **T-DPB** ($5.22 \cdot 10^{-3}$ M) in $\text{CH}_2\text{Cl}_2 + \text{Bu}_4\text{NPF}_6$ 0.2 M, 100 mV.s^{-1} , Pt disk working electrode. Left: 10 recurrent sweeps between -260 and +1740 mV and Right: 10 recurrent sweeps between -370 and +1860 mV.

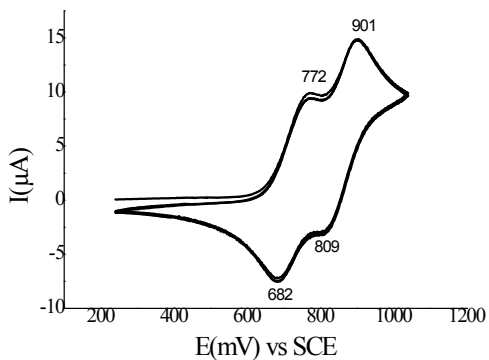


Figure S35. Cyclic voltammogram of **BT-DPB** ($3.95 \cdot 10^{-3}$ M) in $\text{CH}_2\text{Cl}_2 + \text{Bu}_4\text{NPF}_6$ 0.2 M, 100 mV.s^{-1} , Pt disk working electrode. Three recurrent sweeps between 240 and +1040 mV showing the reversibility of the two first oxidation processes.

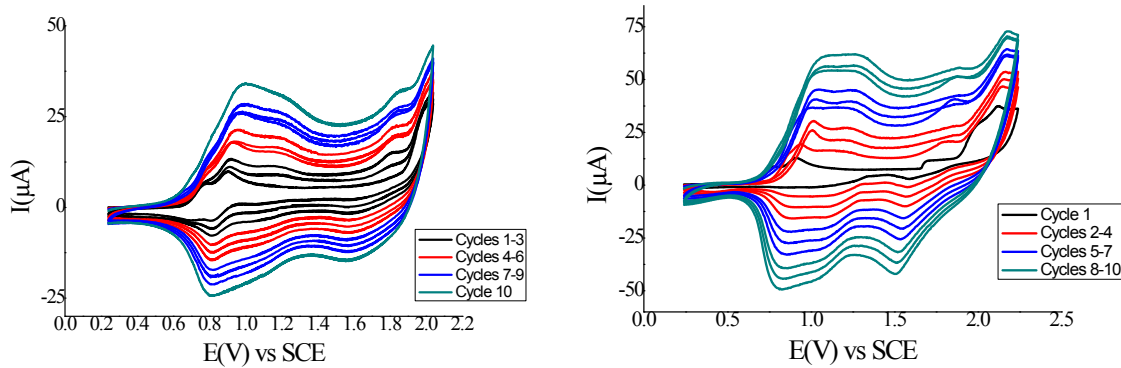


Figure S36. Cyclic voltammogram of **BT-DPB** ($3.95 \cdot 10^{-3}$ M) in $\text{CH}_2\text{Cl}_2 + \text{Bu}_4\text{NPF}_6$ 0.2 M, 100 mV.s^{-1} , Pt disk working electrode. Left: 10 recurrent sweeps between 0.24 and +2.05 V and Right: 10 recurrent sweeps between 0.24 and +2.23 V.

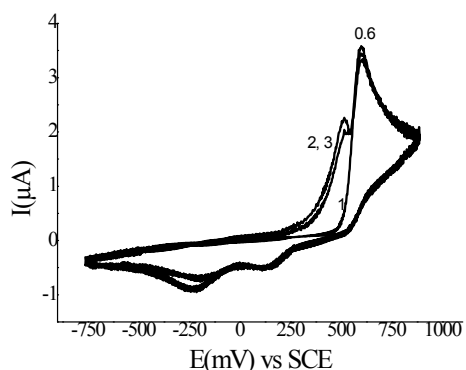


Figure S37. Cyclic voltammogram of **EDOT-DPB** ($3.5 \cdot 10^{-3}$ M) in $\text{CH}_2\text{Cl}_2 + \text{Bu}_4\text{NPF}_6$ 0.2 M, 100 mV.s^{-1} , Pt disk working electrode. Three recurrent sweeps between -760 and +890 mV showing the beginning of electropolymerization since the first oxidation process.

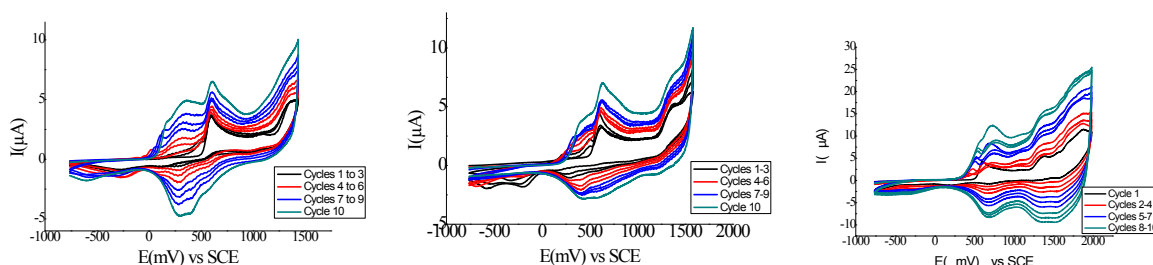


Figure S38. Cyclic voltammogram of **EDOT-DPB** ($3.5 \cdot 10^{-3}$ M) in $\text{CH}_2\text{Cl}_2 + \text{Bu}_4\text{NPF}_6$ 0.2 M, 100 mV.s^{-1} , Pt disk working electrode. Left: 10 recurrent sweeps between -775 and +1430 mV, Middle: 10 recurrent sweeps between -775 and 1600 mV and Right: 10 recurrent sweeps between -775 and 1980 mV.

References

1. L. Palatinus and G. Chapuis, SUPERFLIP. A computer program for the solution of crystal structures by charge flipping in arbitrary dimensions, *J. Appl. Crystallogr.*, 2007, **40**, 786-790.

2. P. W. Betteridge, J. R. Carruthers, R. I. Cooper, K. Prout and D. J. Watkin, CRYSTALS version 12: software for guided crystal structure analysis, *J. Appl. Crystallogr.*, 2003, **36**, 1487.
3. O. V. Dolomanov, L. J. Bourhis, R. J. Gildea, J. A. K. Howard and H. Puschmann, OLEX2: a complete structure solution, refinement and analysis program, *J. Appl. Crystallogr.*, 2009, **42**, 339-341.
4. C. Lee, W. Yang and R. G. Parr, Development of the Colle-Salvetti correlation-energy formula into a functional of the electron density, *Phys. Rev. B: Condens. Matter*, 1988, **37**, 785-789.
5. R. A. Gaussian 09, G. W. T. M. J. Frisch, H. B. Schlegel, G. E. Scuseria, , J. R. C. M. A. Robb, G. Scalmani, V. Barone, B. Mennucci, , H. N. G. A. Petersson, M. Caricato, X. Li, H. P. Hratchian, , J. B. A. F. Izmaylov, G. Zheng, J. L. Sonnenberg, M. Hada, , K. T. M. Ehara, R. Fukuda, J. Hasegawa, M. Ishida, T. Nakajima, , O. K. Y. Honda, H. Nakai, T. Vreven, J. A. Montgomery, Jr., , F. O. J. E. Peralta, M. Bearpark, J. J. Heyd, E. Brothers, , V. N. S. K. N. Kudin, R. Kobayashi, J. Normand, , A. R. K. Raghavachari, J. C. Burant, S. S. Iyengar, J. Tomasi, , N. R. M. Cossi, J. M. Millam, M. Klene, J. E. Knox, J. B. Cross, , C. A. V. Bakken, J. Jaramillo, R. Gomperts, R. E. Stratmann, , A. J. A. O. Yazyev, R. Cammi, C. Pomelli, J. W. Ochterski, , K. M. R. L. Martin, V. G. Zakrzewski, G. A. Voth, , J. J. D. P. Salvador, S. Dapprich, A. D. Daniels, , J. B. F. O. Farkas, J. V. Ortiz, J. Cioslowski, and G. and D. J. Fox, Inc., Wallingford CT, 2009., Gaussian 09, Revision A.02.*Journal*, 2009.